https://dx.doi.org/10.1016/j.conbuildmat.2020.118283



# Effects of sodium/calcium cation exchange on the mechanical properties of calcium silicate hydrate (C-S-H)

Yohannes Lim Yaphary,[a] Denvid Lau,[b] Florence Sanchez,[c] and Chi Sun Poon*[a]

[a] Department of Civil and Environmental Engineering, The Hong Kong Polytechnic University, Hung Hom, Kowloon, Hong Kong

[b]Department of Architecture and Civil Engineering, City University of Hong Kong, Hong Kong, China

[c]Department of Civil and Environmental Engineering, Vanderbilt University, PMB 351831, 2301 Vanderbilt Place, Nashville, TN, 37235-1831, USA

*Correspondence should be addressed to C.S. Poon (email address: cecspoon@polyu.edu.hk)

# Abstract

Calcium silicate hydrate layer (C-S-$H_{layer}$) is considered to be the fundamental building block of hydrated cement. The effect of sodium ions on the atomic scale mechanical properties of C-S-$H_{layer}$ remains, however, unclear. Yet, this information is critical for understanding and predicting the macroscopic performance of concrete structures during their service life. Herein, the intrinsic mechanical properties of C-S-$H_{layer}$ with sodium-exchange ions replacing some calcium cations were studied by molecular dynamics simulations. The interatomic interactions provided insights into the role of $Na^+$ within the atomistic scale of C-S-$H_{layer}$. It was found that $Na^+$ did not significantly alter the mechanical properties (i.e., strength and stiffness) of C-S-$H_{layer}$. The larger cationic attraction on the interlayer water molecules seen in the presence of $Na^+$ occurred due to the exchange of two $Na^+$ for one calcium cation and resulted in a volume expansion of C-S-$H_{layer}$ while a stiffening of its interlayer.



# Keywords

Sodium-exchange cation; portland cement; Calcium silicate hydrate (C-S-H); Mechanical properties; Molecular dynamics simulations


# 1. Introduction

The presence of alkalis (and thus sodium) in concrete can come from various sources, including from the use of admixtures, supplementary cementitious materials, marine resources like seawater and sea sand, as well as from exposure to deicing salts and marine environments. The addition of alkalis (e.g., NaOH and $Na_2SO_4$) during concrete mixing has been reported to affect the mechanical properties of hydrated cement and alite [1-7]. Nevertheless, a fundamental understanding of the effect of the incorporation of sodium ions ($Na^+$) on the mechanical properties of the building block of hydrated cement and the mechanisms by which sodium affects the strength of hydrated cement remains limited. Thus, the present study focused on the effect of $Na^+$ incorporation on the mechanical properties of the building block of hydrated cement.

Hydrated cement is a composite material that mainly consists of calcium silicate hydrates (C-S-H) and possesses a structural hierarchy comprising different components at various scales [8]. At the microscale (scale of capillary and gel pores), C-S-H can be viewed as randomly packed particle clusters (i.e., globules) (Figure 1) [9]. The C-S-H gel consists of clusters (i.e.,

differentiated into low- and high-density C-S-H) of C-S-$H_{globule}$ with gel pores between the globules [10]. At the nanoscale, each C-S-$H_{globule}$ can be viewed as a composite of C-S-H layers (C-S-$H_{layer}$), which constitute the fundamental building block of the hydrated cement. Ultimately, the molecular interactions between the C-S-$H_{layer}$ provide the cohesive forces that bind the hydrated cement into a solid material at the macroscale. C-S-H is primarily responsible for the strength of the hydrated cement paste. Externally applied loads are transferred through the hydrated cement and C-S-H at various scales. At the scale of capillary and gel pores, externally applied loads are transferred into the clusters of C-S-H globules that maintain their integrity through cohesive forces between them. The loads exerted onto the C-S-H globules are, in turn, transferred to the composite layers of C-S-H. Sodium has been reported to sorb onto the C-S-H phases and replace some of the calcium within the C-S-$H_{layer}$ [11-13]. This cation exchange process may affect the molecular interactions in C-S-$H_{layer}$ and thus impact the mechanical properties of C-S-H. A further understanding of the effect of sodium on the strength of the hydrated cement thus relies heavily on the appropriate understanding of the strength of the modified C-S-$H_{layer}$.

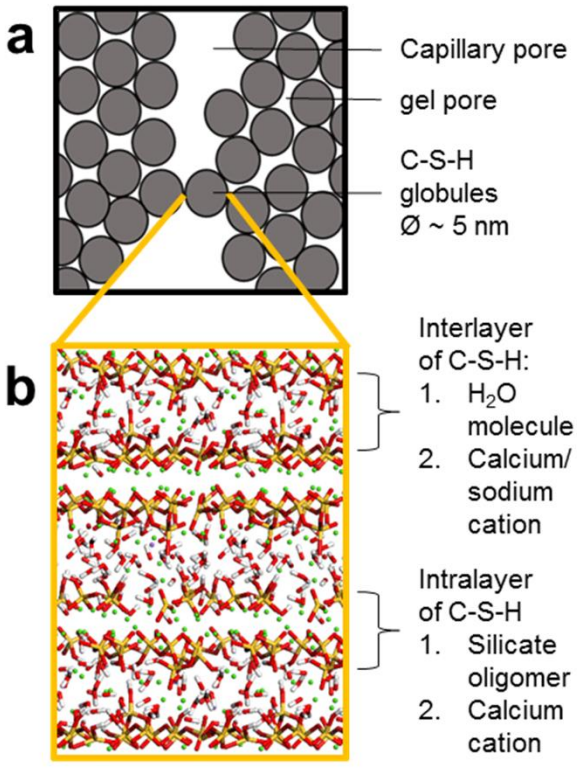

Figure 1. Hierarchical structure of hydrated cement: (a) microscale level is comprised of capillary pores, gel pores, and clusters of C-S-H globules and (b) C-S-H globules are comprised of composite layers of C-S-H (C-S-$H_{layer}$) [14].

Experimental techniques such as atomic force microscopy and nanoindentation mapping are effective methods to study the mechanical properties of C-S-H especially its stiffness at the micro-scale level [15-17]. However, these techniques cannot offer insights into the mechanical properties at the scale below the micro-level due to technical limitations such as the size of the indenter tip [18] and thus cannot probe the mechanical properties of C-S-$H_{layer}$. Atomistic simulations are powerful techniques that complement experimental methods for studying hydrated cement down to the fundamental scale (i.e., interatomic interactions) [19-24]. Molecular dynamics (MD) simulations have been successfully used in the literature to study the adsorption of $Na^+$ cations into C-S-$H_{layer}$ and have indicated that the adsorption of $Na^+$cations can lead to a reduction of *ca*. 5% of the elastic modulus of the C-S-$H_{layer}$ under loading along the direction that was perpendicular to C-S-$H_{layer}$ and to a volume expansion of *ca*. 0.25% [25]. However, the information reported in the literature on the effect of $Na^+$ are limited only to the elastic modulus of C-S-$H_{layer}$. The effect of $Na^+$ on the strength of C-S-$H_{layer}$ and the underlying atomistic mechanisms of the mechanical response of C-S-$H_{layer}$ remain poorly understood. Yet, the strength of hydrated cement is directly related to its failure resistance under loading. Furthermore, $Na^+$ may differently influence the mechanical properties of C-S-$H_{layer}$ depending on the direction of the applied load (i.e., along the direction that is perpendicular or parallel to the C-S-$H_{layer}$).

The objective of this study was to investigate the change in the mechanical properties of C-S-$H_{layer}$ with the incorporation of $Na^+$ to replace $Ca^{2+}$. More specifically, MD simulations were performed to determine the difference in compressive and tensile strengths of C-S-$H_{layer}$ with and without the incorporation of $Na^+$. The stiffness under the applied load along the direction parallel to C-S-$H_{layer}$ was also determined. Additionally, the relative behavior of the atoms in the structure (i.e., average per-atom stress) as a response to an externally applied load was examined as a function of strain in the longitudinal (z) and lateral (xy) directions for compressive and tensile loadings along the z-direction. The findings from this study provide useful information for the strategic use of cementitious material in sodium rich environments.

# 2. Atomistic simulations

## 2.1. Model

The unit cell of C-S-$H_{layer}$ used in the study followed the model developed by Pelleng et. al. [26] and based on modification of tobermorite-11 Å. The modification included the presence of water molecules and the reconstruction of the silicate structure into short oligomers silica (i.e., distributed as monomers, dimers, and pentamers). The assumption made to reconstruct the silicate structure was based on experimental results reported in the literature using 29Si nuclear magnetic resonance (NMR) [27, 28]. The resulting model of C-S-$H_{layer}$ was found to describe well both the experimental chemical-composition of $(CaO)_{1.65}(SiO_2)(H_2O)_{1.75}$ and its density [29].

Results from the literature were used to model the C-S-$H_{layer}$ with the incorporation of $Na^+$ into its structure [12, 25]. It has been reported that the stoichiometry of C-S-H (i.e., Ca/Si~1.7) obtained from alite (impure tricalcium silicate) was not significantly affected by the use of sodium hydroxide (NaOH) present in the mixing water [1]. Additionally, semi-grand canonical Monte Carlo simulations have indicated that two $Na^+$ cations can be adsorbed in the C-S-H hydrated interlayer with each calcium cation replaced by $Na^+$ cations when the $Na^+$ concentration was up to 0.1 mol/kg of C-S-H [25]. Furthermore, the amount of calcium released from C–S–H and the amount of adsorbed sodium on C–S–H has been shown to be linearly related with a slope of approximately 0.5, suggesting that 2 mol of sodium were adsorbed onto C–S–H by replacing 1 mol of calcium [12]. The size of the C-S-$H_{layer}$ supercell was thus selected to accommodate the adsorption of $Na^+$ at a concentration of 0.1 mol/kg. The C-S-H supercell was made by doubling the C-S-H unit cell (i.e., ~ 13 Å × 18 Å × 24 Å) in the x, y and z directions. The created C-S-H supercell was ~ 26 Å × 36 Å × 48 Å and consisted of four intra- and interlayers as shown in Figure 2. The C-S-H with $Na^+$ was made by replacing one calcium (i.e., at the center) in each interlayer with two $Na^+$ to keep the charges neutral. The supercells of C-S-$H_{layer}$ with and without $Na^+$ were named C(Na)-S-H and C(Ca)-S-H, respectively.

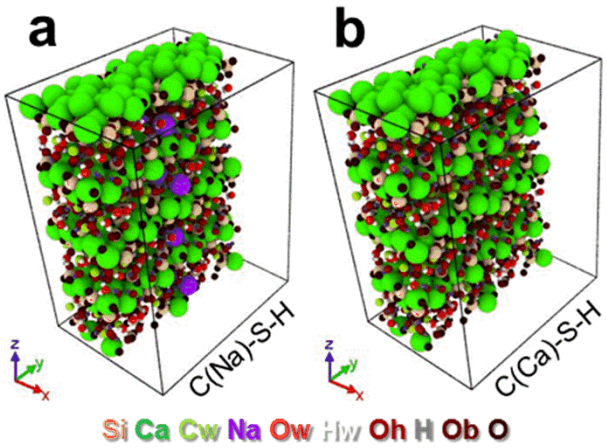


Figure 2. Supercells of (a) C(Na)-S-H and (b) C(Ca)-S-H models with dimensions of ~ 26 Å × 36 Å × 48 Å. Only half of the atoms of the supercells are presented (i.e., the other half is hidden) to show the presence of $Na^+$ in the C-S-$H_{layer}$ supercell. [Si: Silicon; Ca: Intralayer calcium; Cw: Interlayer calcium; Na: Sodium-exchange cation ($Na^+$); Ow: Water oxygen; Hw: Water hydrogen; Oh: Oxygen (formally carrying a H atom); H: Hydrogen; Ob: End oxygen; O: Bridging oxygen].

## 2.2. Interatomic interaction

The Calcium Silicate Hydrates Force-Field (CSH FF) [30] was employed for the simulations of the C-S-H. CSH FF is based on the Clay Force Field (ClayFF) [31] and was developed to model hydrated calcio-silicates without using a core-shell description, which is time-consuming. Assuming equal CPU resources, CSH FF has been shown to be 3.4 times more efficient than a core–shell model in terms of computational time for energy minimization, which scales to $N^3$ (i.e., N is the number of atoms in the system) [31]. CSH FF has been demonstrated to successfully improve the predictive capabilities of ClayFF when applied to the C-S-H model developed by Pelleng et al. [26, 32-35].

The calculation of the potential energy using CSH FF is based on Equation 1 [30] which includes non-covalent and covalent interactions. Non-covalent bonds are consisted of van der Waals ($1^{st}$ term) and short-range Coulombic electrostatic ($2^{nd}$ term) interactions. The van der Waals interaction is represented as a conventional 12-6 Lennard-Jones function. Covalent bonds are consisted of bond stretch ($3^{rd}$ term) and angle bend ($4^{th}$ term), both of which are considered harmonic.

$$E_p = 4\varepsilon\left[\left(\frac{\sigma}{r}\right)^{12} - \left(\frac{\sigma}{r}\right)^{6}\right] + \frac{Cq_iq_j}{\varepsilon_r r} + K(r - r_0)^2 + K(\theta - \theta_0)^2 \quad (1)$$

In Equation 1, ε is the depth of the potential well, σ is the finite distance at which the inter-atom potential is zero, r is the distance between the atoms, C is an energy-conversion constant, $q_i$ and $q_j$ are the charges on the atoms, $\varepsilon_r$ is dielectric constant, K is a constant, $r_0$ is the equilibrium bond distance and $\theta_0$ is the equilibrium value of the angle. The CSH FF parameters can be found in the existing literature [25, 30].

## 2.3. Dynamic evolution

MD simulations were performed using LAMMPS (Large-scale Atomic/Molecular Massively Parallel Simulator), which is a well-tested and widely used open source classical molecular dynamics code [36]. In the simulation, a Nosé−Hoover thermostat and barostat were used to control the temperature and pressure, respectively (independently in the x-, y-, and z-directions) [37-39]. Short-range interactions were truncated at 12 Å and long-range electrostatic interactions were computed using the Ewald summation with an accuracy of $10^{-4}$ [30]. This accuracy is a unitless value that is used in parameterization of the long-range solver of Ewald summation so the root-mean-square (RMS) error (i.e., between the exact force and the approximated force calculated by using the long-range solver) is $10^4$ smaller than the reference force (i.e., the force that two unit points, each with a single charge, exert on each other at a distance of 1 Å) [40]. Different simulation schemes were used to study the dimensional properties (i.e., volume and density changes) and mechanical properties of C(Na)-S-H (with $Na^+$) and C(Ca)-S-H. To examine the dimensional properties, the simulations were performed in the isobaric-isothermal ensemble (i.e., NPT, constant number of particles N, pressure P, and temperature T) using a constant pressure of 1 atm and a temperature of 300 K. A time step of 0.1 fs was used and periodic boundary conditions were applied in all directions. The stage of equilibration was run for 1 ns. The potential energy and root-mean-square displacement (RMSD) of the atoms were monitored as a function of time until steady state was achieved to ensure equilibrium. After the stage of equilibration, the dimensional properties of C-S-H were collected over 0.1 ns.

The compression and tensile properties of C(Na)-S-H and C(Ca)-S-H were determined as an average of three measurements using NPT ensemble conditions at 300 K and 0 atm after 1, 1.2 and 1.4 ns of equilibration. The equilibrium was also determined based on the steady state potential energy and RMSD. A time step of 0.01 fs was used and periodic boundary conditions were applied in all directions. Uniaxial deformations were performed along the x-, y- and z-directions. While performing the deformation along one direction, the pressure along the other two directions was maintained at zero to allow for Poisson's effect. The non-pressure setting in the directions perpendicular to the loading direction was used to eliminate the artificial constrain for the deformation and allow the free development of tension without any restriction [41]. The strain rate used for the simulations was determined based on considerations of changes in the stress-strain profile, simulation cost, and comparison of results of mechanical properties from previous studies found in the literature. The Young's modulus was calculated from the slope of the stress-strain plot [42]. The best linear fit was determined from the group of stress-strain data with strain increments of ±0.01 (i.e., within the linear portion of the stress-strain plot) that had an optimum $R^2$. The mechanical properties along the xy-direction were calculated as the average of the mechanical properties along the x- and y-directions.

To provide insights into the atomic response of C-S-$H_{layer}$ and the role of $Na^+$ upon externally applied loads, the average per-atom stress was determined in the longitudinal and lateral directions for compression and tensile loadings along the z-direction. The per-atom stress ($P_a$) from a kinetic and virial contribution was calculated using Equation 2, where *a* takes on value of x, y and z to generate the pressure on atom *i* along the x-, y- and z- directions [43]. The per-atom volume ($V_a$) was calculated based on Voronoi tessellation of the atoms in the simulation box [44]. The 1st term of Equation 2 is a kinetic energy contribution from atom *i*. The *r* and *F* are the position and acting force of the atom, respectively. The virial contribution on the per-atom potential energy is calculated from the 2nd to 5th term. The 2nd term is a pairwise energy contribution on atom *i* due to its interaction with neighbouring atoms. The 3rd and 4th term is the bond and angle energy contribution which atom *i* is a part of. The 5th term accounts for the energy contribution from long-range coulombic interactions of atom *i* [45] . The *n* in the 2nd, 3rd and 4th terms loops over the $N_p$ neighbours, $N_b$ bonds and $N_a$ angles of atom *i*, respectively.

$$P_a = -\frac{1}{V_a}\left[m{v_a}^2 + \frac{1}{2}\sum_{i,j=1}^{N_p}\left(r_{ia}F_{ia} + r_{ja}F_{ja}\right) + \frac{1}{2}\sum_{i,j=1}^{N_b}\left(r_{ia}F_{ia} + r_{ja}F_{ja}\right) + \frac{1}{3}\sum_{i,j,k=1}^{N_a}\left(r_{ia}F_{ia} + r_{ja}F_{ja} + r_{ka}F_{ka}\right) + K_{space}(r_{ia}, F_{ia})\right] \quad (2)$$

# 3. Result and discussion

## 3.1. Volumetric change

Figures 3a and 3b show the atom configuration of C(Na)-S-H (with $Na^+$) and C(Ca)-S-H, respectively after 1 ns of equilibration. As shown in Figure 3c, a greater volume was found for C(Na)-S-H compared to C(Ca)-S-H, corresponding to *ca*. 0.6% expansion. This expansive effect of $Na^+$ was consistent with a previous study in the literature, which reported *ca*. 0.25% expansion for different Ca/Si C-S-$H_{layer}$ in the presence of sodium cations [25]. Furthermore, the greater volume of C(Na)-S-H was consistent with the observed swelling of hydrated cement and C-S-H in the presence of sodium chloride [46] and provided further insights into the mechanisms of swelling in the presence of sodium. The expansion of the C-S-$H_{layer}$ caused by the incorporation of $Na^+$ was thought to be, in turn, observable at the macroscale and, thus, intrinsic to the swelling of hydrated cement in the presence of sodium.

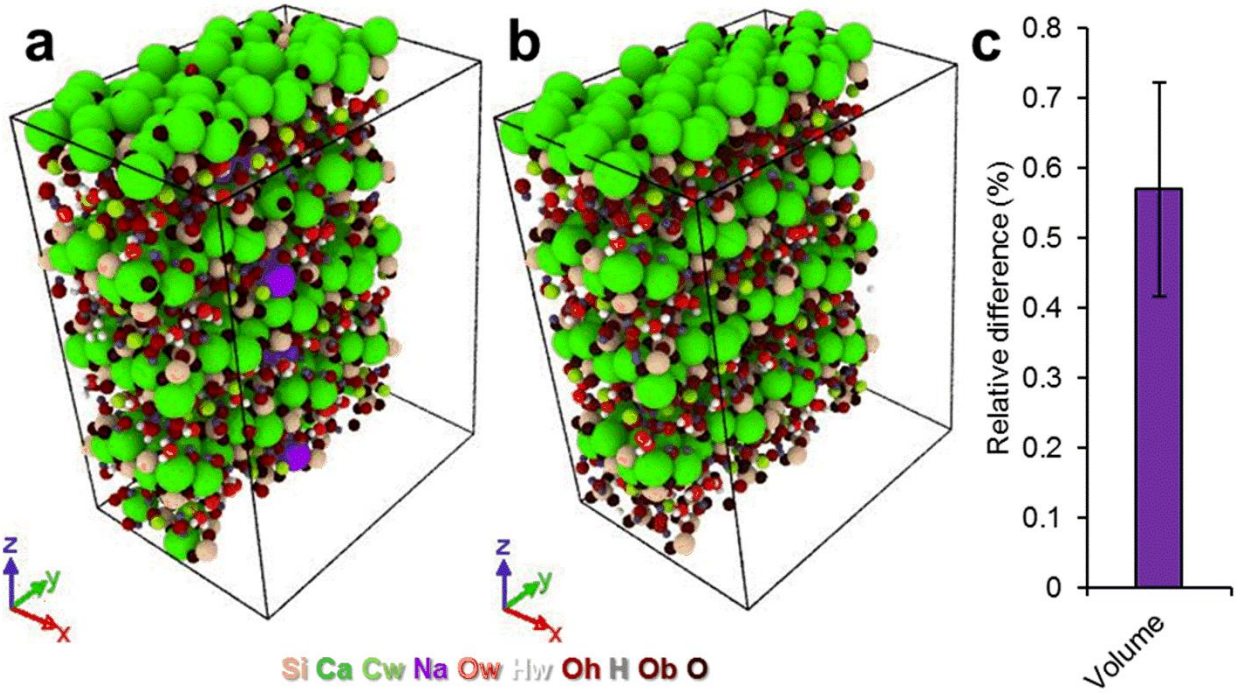

Figure 3. Equilibrium snapshots from MD simulations under NPT ensemble at 300 K and 1 atm of the C-S-$H_{layer}$ (a) with $Na^+$ (C(Na)-S-H) and (b) without $Na^+$ (C(Ca)-S-H). (c) Changes in volume of C(Na)-S-H relative to C(Ca)-S-H.

Figure 4 shows the dimensional change in the z- and xy-directions. Although the volume of C(Na)-S-H (with $Na^+$) was larger than that of C(Ca)-S-H, the increase in dimensions did not occur in all direction. The cross-sectional area in the xy-direction parallel to the C(Na)-S-H was decreased while the length in the direction perpendicular to the C(Na)-S-H was increased. These observations indicated that the presence of $Na^+$ in the interlayer of C(Na)-S-H decreased the cross-sectional area of the C-S-$H_{layer}$ but increased the thickness of the interlayer. The dimensional change observed in the presence of $Na^+$ was thought to be caused by the greater attraction of two $Na^+$ (compared to one calcium cation) for the water molecules [47]. The $Na^+$ attracted the water molecule along the direction that was parallel to the C(Na)-S-H. The force resulting from this attraction decreased the lateral area (i.e., along the xy-direction), while simultaneously increased the length along the z-direction (i.e., expanded the interlayer).

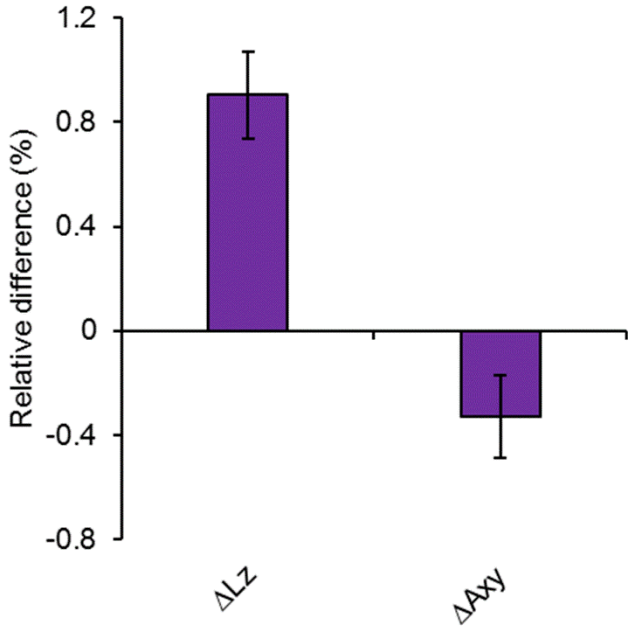


Figure 4. Relative difference in length (z-direction) and cross-sectional area (xy-direction) of C(Na)-S-H (with $Na^+$) and C(Ca)-S-H.

## 3.2. Effect of strain rate on strength characteristics of C-S-$H_{layer}$

The effect of strain rate on the compressive and tensile stress-strain profiles is shown in Figures 5 and 6, respectively. There was no distinctive failure mode of C-S-$H_{layer}$ under different compressive strain rates as can be seen in Figure 5. However, a distinct failure mode (Figure 6b) could be observed under different tensile strain rates. The highest strain rate tested ($10^{-3}$ $fs^{-1}$) resulted in the greatest ultimate compressive and tensile strengths. Lower compressive and tensile failure strains were observed with the use of lower strain rates.

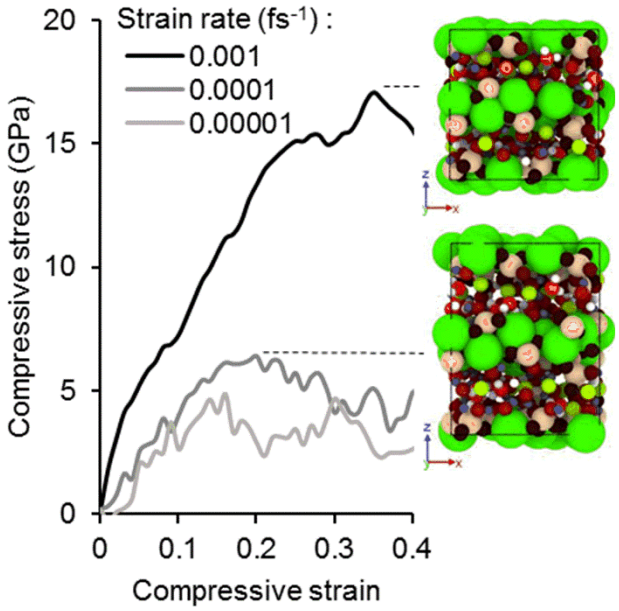


Figure 5. Effect of strain rate on the stress-strain profile of C-S-$H_{layer}$ under compressive loading.

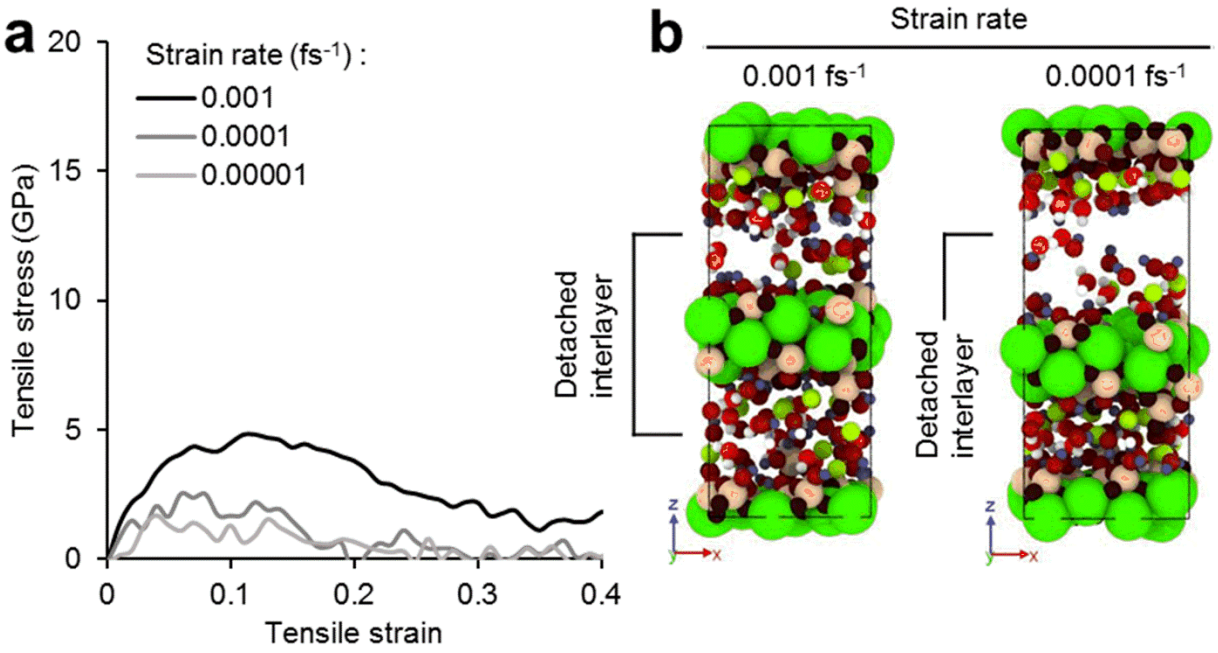


Figure 6. (a) Effect of strain rate on the stress-strain profile of C-S-$H_{layer}$ under tensile loading. (b) Failure mode of C-S-$H_{layer}$ under two different tensile strain rates (i.e., $10^{-3}$ $fs^{-1}$ and $10^{-4}$ $fs^{-1}$), showing detachment of each interlayer for the strain rate of $10^{-3}$ $fs^{-1}$ while only of the top layer for the strain rate of $10^{-4}$ $fs^{-1}$.

Although there was an influence of the strain rate on the compressive and tensile strengths of C-S-H, the effect became smaller for smaller strain rates (i.e., from $10^{-4}$ $fs^{-1}$ to $10^{-5}$ $fs^{-1}$). Considering the simulation cost, the strain rate of $10^{-4}$ $fs^{-1}$ was therefore used thereafter to study the strength of C(Na)-S-H (with $Na^+$) and C(Ca)-S-H. The use of a strain rate of $10^{-4}$ $fs^{-1}$ provided similar compressive and tensile strengths of C(Ca)-S-H to that reported in the literature [41]. Furthermore, the compressive Young's modulus of *ca.* 46 GPa from the stress-strain profile of C-S-$H_{layer}$ with the strain rate of $10^{-4}$ $fs^{-1}$ was similar to the nanoindentation modulus of ultra-high-density (UHD) C-S-H (i.e., *ca.* 49 ± 3 GPa) [48]. Therefore, it was considered that the use of a strain rate of $10^{-4}$ $fs^{-1}$ could adequately capture the mechanical properties of C-S-$H_{layer}$.

## 3.3. Compressive and tensile strengths of C(Na)-S-H and C(Ca)-S-H

Figure 7 shows the stress-strain profiles of C-S-$H_{layer}$ under compressive and tensile loadings. The strain-stress profiles of C(Na)-S-H (with $Na^+$) and C(Ca)-S-H were overall similar. The

significance of the difference in mechanical properties between C(Na)-S-H and C(Ca)-S-H was evaluated by the t-test using a significance level of 0.05 (confidence level of 95%).

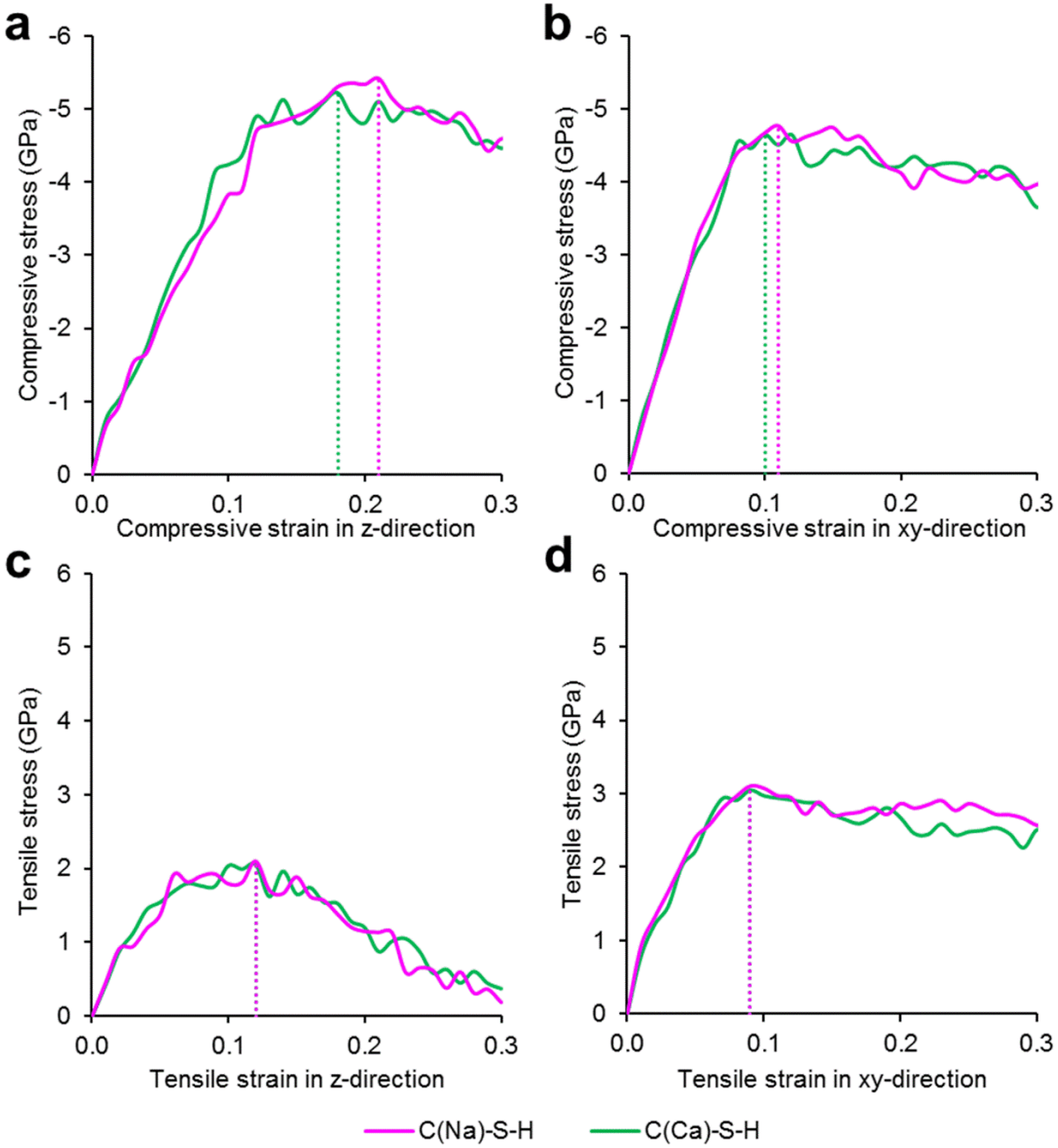


Figure 7. Average strain-stress profile of C(Na)-S-H (with $Na^+$) and C(Ca)-S-H under compression in (a), (b) z- and xy-directions, respectively and under tensile in (c), (d) z- and xy-directions, respectively.

Figure 8 shows the comparison of the Young's modulus, ultimate compressive and tensile strengths, and fracture strains of the C-S-$H_{layer}$ with and without $Na^+$. The lower tensile strength of C(Ca)-S-H (without $Na^+$) under loading along the z-direction compared to the xy-direction agreed with previously reported simulation results reported in the literature [18], which also found a lower tensile strength of the C-S-$H_{layer}$ along the z-direction. The results further indicated that a lower tensile strength also occurred for C(Na)-S-H (with $Na^+$). In addition, the compressive strength was found to be higher under loading along the z-direction than under the xy-direction. The Young's moduli of C-S-$H_{layer}$ obtained in the current study were all within the range of reported elastic moduli from the literature (Figure 9). However, the effect of $Na^+$ on the mechanical properties was statistically insignificant at the 95% confidence level as indicated by the t-test that showed p-values above 0.05 for all cases. This result differed from the nanoindentation results reported in the literature that have shown an increase in the nanoindentation modulus of C-S-H formed in the presence of sodium. For example, the average of nanoindentation modulus of hydrated alite with NaOH [49] and hydrated cement with NaCl [50] has been reported to be higher than that of plain hydrated alite and cement. It should be recalled that hydrated cement is a composite material with structural hierarchy (Figure 1). When comparing the mechanical properties of hydrated cement determined from experimental testing (nanoindentation) and simulations, caution should be made in terms of scale. Also, the accompanying anions of the sodium containing compounds should be considered. These results suggested that the effect of sodium ion on the mechanical properties of hydrated cement most likely does not originate from the atomic level of C-S-$H_{layer}$. This was furthermore consistent with the results from Mendoza et al. [49] who attributed the increase in nanoindentation modulus of C-S-H (i.e., produced from alite hydration with NaOH) to the electrostatic attraction between the positively charged sodium cation and the negatively charged C-S-H.

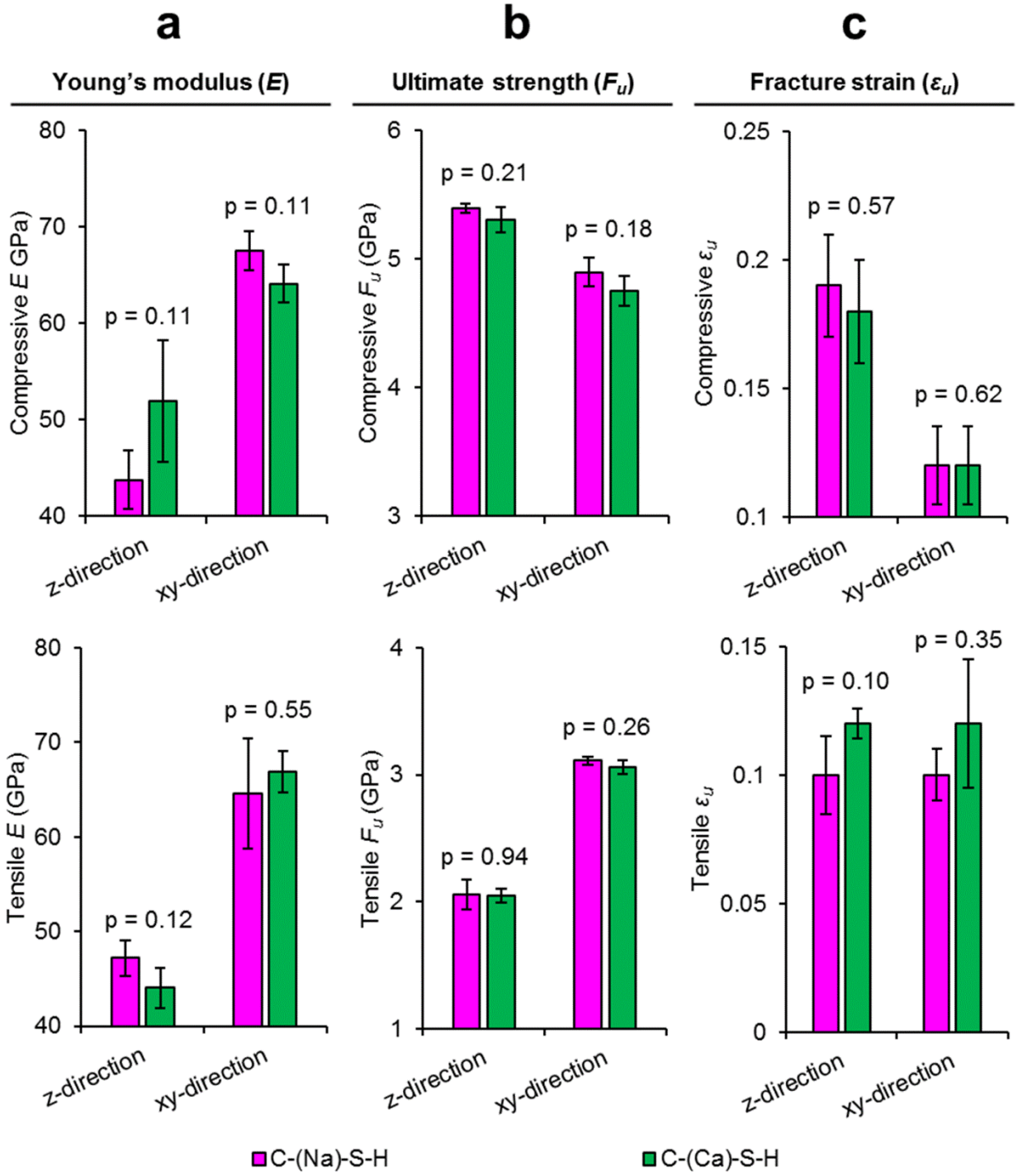


Figure 8. (a) Young's modulus, (b) ultimate strength, and (c) fracture strain of C(Na)-S-H (with $Na^+$) and C(Ca)-S-H under compressive (top) and tensile (bottom) loadings. Na and Ca indicate C(Na)-S-H and C(Ca)-S-H, respectively. p is the t-test probability of difference between the mechanical properties of C(Na)-S-H and C(Ca)-S-H.

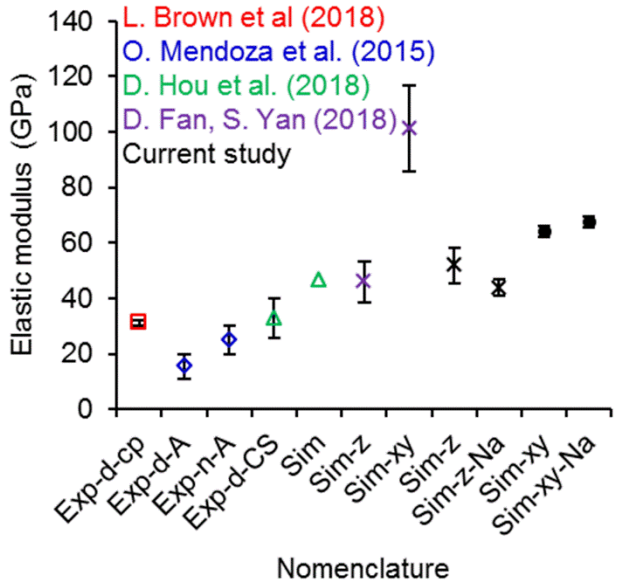


Figure 9. Comparison of the elastic modulus of C-S-H determined by nanoindentation (i.e., nanoindentation modulus) [49, 51, 52] and molecular dynamics simulations (i.e., Young's modulus) [52, 53]. [Exp: experimental; Sim: simulation; d: distilled water; n: NaOH solution; cp: cement paste; A: alite; CS: $C_3S$; Na: sodium-exchange cation; z and xy: compressive loading along the direction perpendicular and parallel to the C-S-$H_{layer}$, respectively.]

The information obtained regarding the effect of $Na^+$ on the mechanical properties of C-S-$H_{layer}$ provided new insights into the durability of concrete structures. While it is generally considered that saline environments have adverse effects on the durability of concrete structures [54, 55], the MD simulation results showed that the effect of $Na^+$ was not detrimental to the mechanical properties of C-S-$H_{layer}$ (the strength of C-S-$H_{layer}$ was slightly increased by the presence of $Na^+$). However, it should be noted also that the swelling of C-S-$H_{layer}$ resulting from the presence of $Na^+$ can also induce stresses on the hardened hydrated cement. The coupled effect of $Na^+$ on the swelling and strength of the C-S-$H_{layer}$ should thus be taken into consideration.

## 3.4. Atomistic response of C-S-H layers to externally applied loads

Under compressive loading (Figure 10), the average per-atom stress of all atoms in the longitudinal (z) direction had a negative sign, except for the hydrogen atoms (i.e., from water and non-water molecules: Hw and H, respectively), indicating that most of the atoms located in the interlayers

experienced compression. In the lateral (xy) direction, however, most of the atoms located in the intralayers experienced tensile stresses (positive sign) during compressive loading. The opposite behavior was observed when tensile loading was applied along the z-direction (Figure 11) with the atoms experiencing tension in the longitudinal direction and compression in the lateral direction.

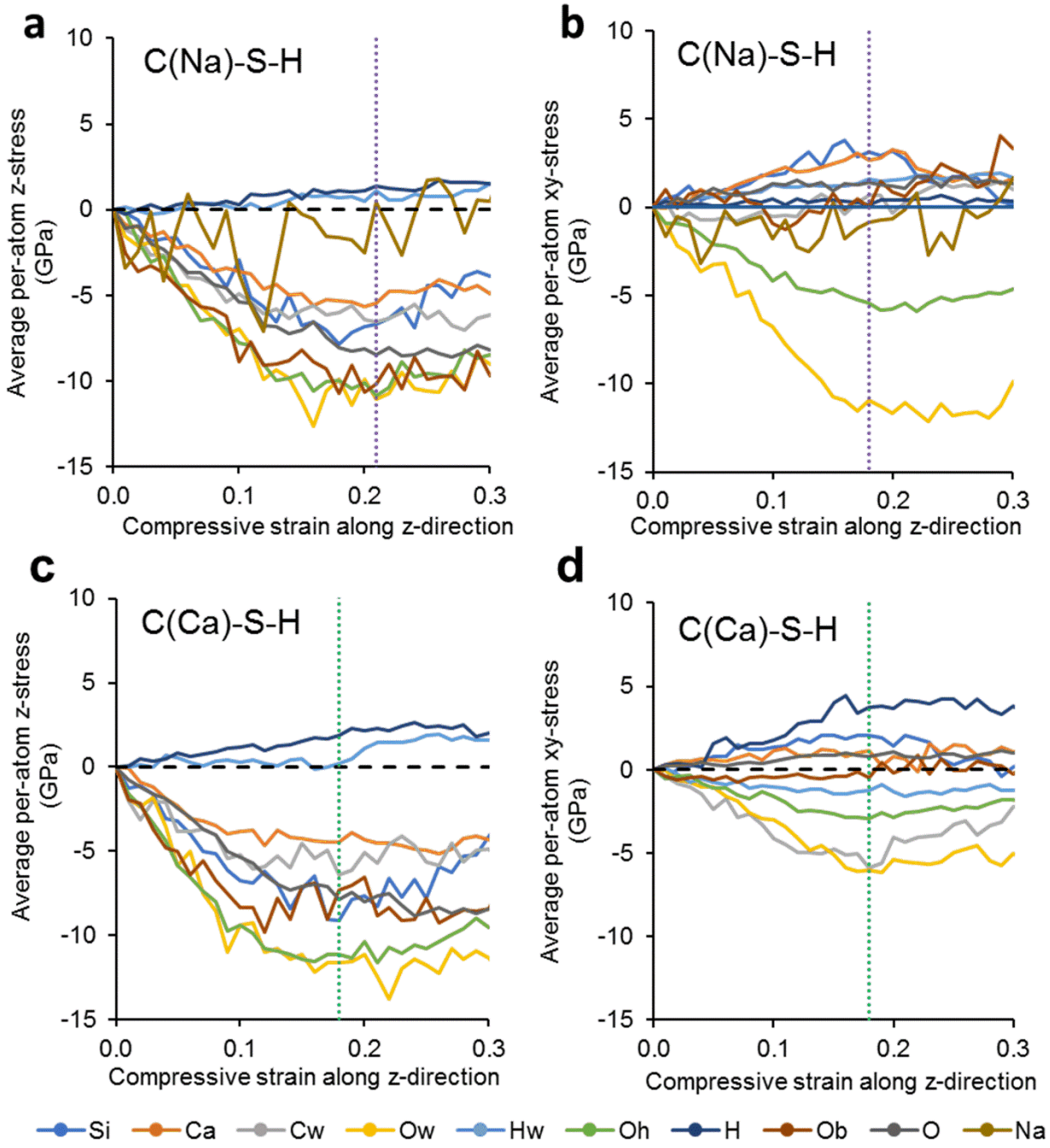

Figure 10. Evolution of the average per-atom stress during compressive loading along the z-direction: (a) and (c) longitudinal (z-pressure) direction for C(Na)-S-H (with $Na^+$) and C(Ca)-S-H, respectively and (b) and (d) lateral (xy-pressure) direction for C(Na)-S-H and C(Ca)-S-H, respectively. The negative and positive signs indicate compression and tension, respectively. The vertical dot lines indicate the strain at the maximum (ultimate) compressive strength. [Si: Silicon; Ca: Intralayer calcium; Cw: Interlayer calcium; Na: Sodium-exchange cation; Ow: Water oxygen; Hw: Water hydrogen; Oh: Oxygen (formally carrying a H atom); H: Hydrogen; Ob: End oxygen; O: Bridging oxygen].

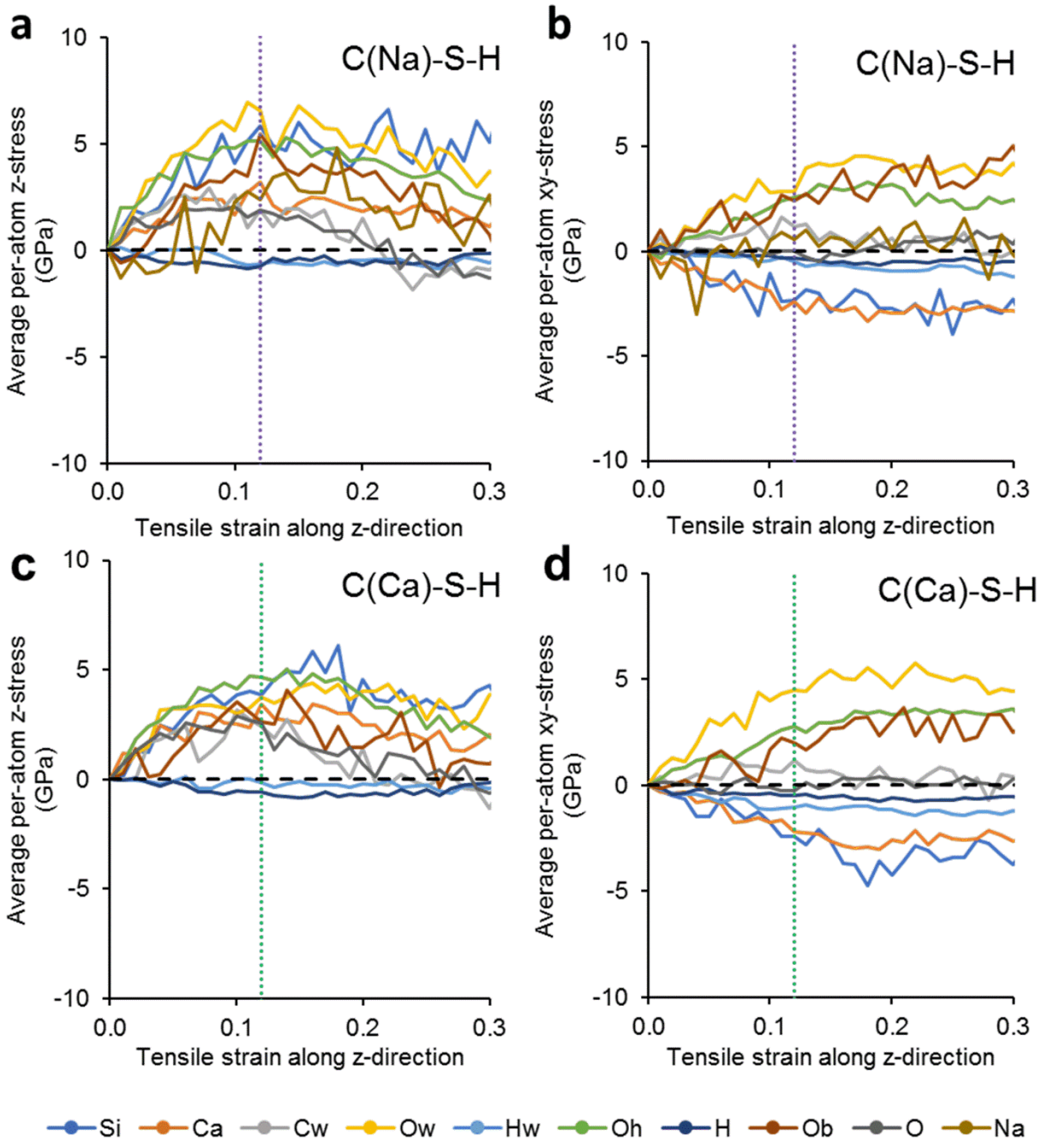


Figure 11. Evolution of the average per-atom stress during tensile loading along the z-direction: (a) and (c) longitudinal (z-pressure) direction for C(Na)-S-H (with $Na^+$) and C(Ca)-S-H, respectively and (b) and (d) lateral (xy-pressure) direction for C(Na)-S-H and C(Ca)-S-H, respectively. The negative and positive signs indicate compression and tension, respectively. The vertical dot lines indicate the strain at the maximum (ultimate) tensile strength.

Classification of the atoms of C-S-$H_{layer}$ based on their response to externally applied loads provided insights into the load carrying mechanisms of C-S-$H_{layer}$ and was used to simplify the model of C-S-$H_{layer}$ into a bilayer (i.e., inter- and intralayer) composite as illustrated in Figure 12. The representation of C-S-$H_{layer}$ as a bilayer system can be a useful approach in a bottom-up strategy to model the mechanical response of C-S-$H_{layer}$ to externally applied loads. Based on the simulation results, in the longitudinal (z) direction, the stressed atoms responded by transferring the externally applied loads (compressive or tensile) to the neighbouring atoms and created longitudinal deformation. Simultaneously, the longitudinal deformation exerted a lateral load and induced lateral pressure. The similar pressure values (*i.e.,* compression and tension) between the per-atom stress and the externally applied load indicated that the atoms in the interlayer transferred the externally applied load along the lateral direction. The opposite stress between the per-atom stress and the externally applied load implies that the atom in the intralayer resisted the lateral deformation.

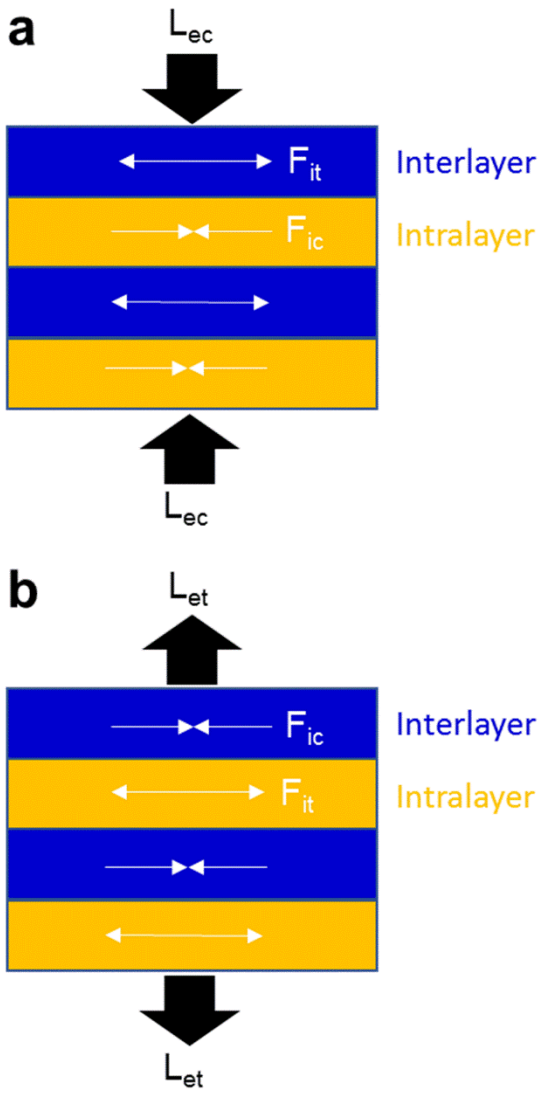


Figure 12. Simplified model of C-S-$H_{layer}$ as bilayer composite under (a) compressive and (b) tensile loadings. $L_{ec}$ and $L_{et}$ are externally applied compressive and tensile loads, respectively. $F_{ic}$ and $F_{it}$ are internally lateral compressive and tensile forces as a response to the externally applied loads, respectively.

In the presence of $Na^+$, the oxygen and hydrogen atoms of water (i.e., Ow and Hw) of the interlayer behaved differently under compressive and tensile deformations along the perpendicular direction (z-direction) of the C-S-$H_{layer}$ (Figure 13a). Under compressive deformation, the average per-atom lateral compressive stress of the water atoms (i.e., Ow and Hw) of the interlayer in C(Na)-S-H was higher than those of the atoms in C(Ca)-S-H (as indicated by a pressure ratio greater than

1), which was due to the attraction of the water molecules by $Na^+$. The reverse was, however, observed under tensile deformation, as shown in Figure 13a, with a ratio that was then less than 1. Concurrently, in the intralayer, the average per-atom lateral tensile stress of the calcium cations under compressive loading decreased because of the influence of $Na^+$ attraction as can be seen in Figure 13b. This attraction stiffened the structure in the intralayer of C-S-$H_{layer}$ and resisted the movement of water along the lateral deformation. Hence the load that was transferred to the intralayer calcium decreased. In addition, the attraction of the water molecules by $Na^+$ affected the molecular structure of the C-S-$H_{layer}$ in term of its volume (i.e., larger volume of the C-S-$H_{layer}$ in the presence of Na+). Furthermore, the stiffening effect of the intralayer of the C-S-$H_{layer}$, resulting from the additional water molecules attracted by $Na^+$, caused comparable mechanical properties between C(Na)-S-H and C(Ca)-S-H even though C(Na)-S-H had a higher volume (i.e., less dense) than C(Ca)-S-H.

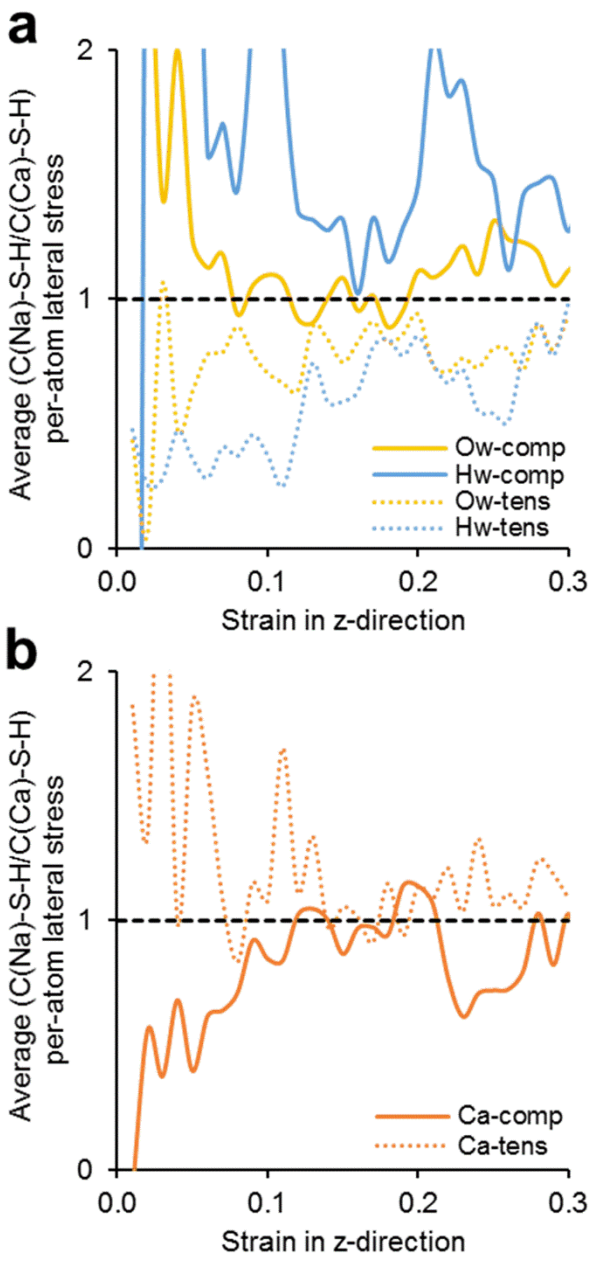


Figure 13. Ratio of the average per-atom lateral stress of (a) Ow and Hw atoms from the water molecules and (b) intralayer calcium atoms between C(Na)-S-H and C(Ca)-S-H under compressive (i.e., full line) and tensile (i.e., dot line) loadings. [Ow: Water oxygen; Hw: Water hydrogen; Ca: Intralayer calcium; comp: compressive loading; tens: tensile loading].

## 3.5. Attractive force of sodium-exchange cation in C-S-$H_{layer}$

Figure 14 shows the radial distribution function between the oxygen and hydrogen atoms of the water molecules (i.e., Ow and Hw) and the calcium (Cw) and sodium ($Na^+$) cations in the interlayer of C-S-$H_{layer}$ for C(Na)-S-H (with $Na^+$) and C(Ca)-S-H. The attraction of water oxygen by the calcium cations was greater than that by the sodium cations (Figure 14a). In contrast, the attraction of water hydrogen was greater for the sodium cations (Figure 14b). The attraction of water oxygen (i.e., as compared to water hydrogen) toward cations gave a more indicative measure of the water attracting effect by the cations. Cations such as sodium and calcium tend to attract and orient the water molecules around them (i.e., the more negative side of the oxygen atom of the water molecule is oriented towards cations) [56, 57]. Therefore, Figure 14a implies that the attraction of sodium on the water molecule was less than calcium. The water attracting effect by sodium and calcium agreed with the hydration numbers of sodium and calcium cations, which are 4 and 6, respectively [58]. The replacement of one calcium cation by two $Na^+$ cations resulted in a greater water attracting effect for both the short- and long-range interactions. For the short-range interactions (i.e., within the first-shell perimeter, ~4 Å into the cation), the greater water attracting effect could be associated with the larger total hydration number of two $Na^+$. For the long-range interactions, the greater attracting effect was caused by the relatively greater attractive potential-energy of 2Na-Ow compared to Ca-Ow as shown in Figure 15. The greater water attracting effect of the short- and long-range $Na^+$-water interactions resulted in a stiffening of the interlayer of C-S-$H_{layer}$, which explained the decrease in lateral dimension and the change in magnitude of per-atom lateral stress (i.e., reduction in the per-atom lateral stress of calcium cation at the intralayer of C-S-$H_{layer}$ under longitudinal compressive loading.

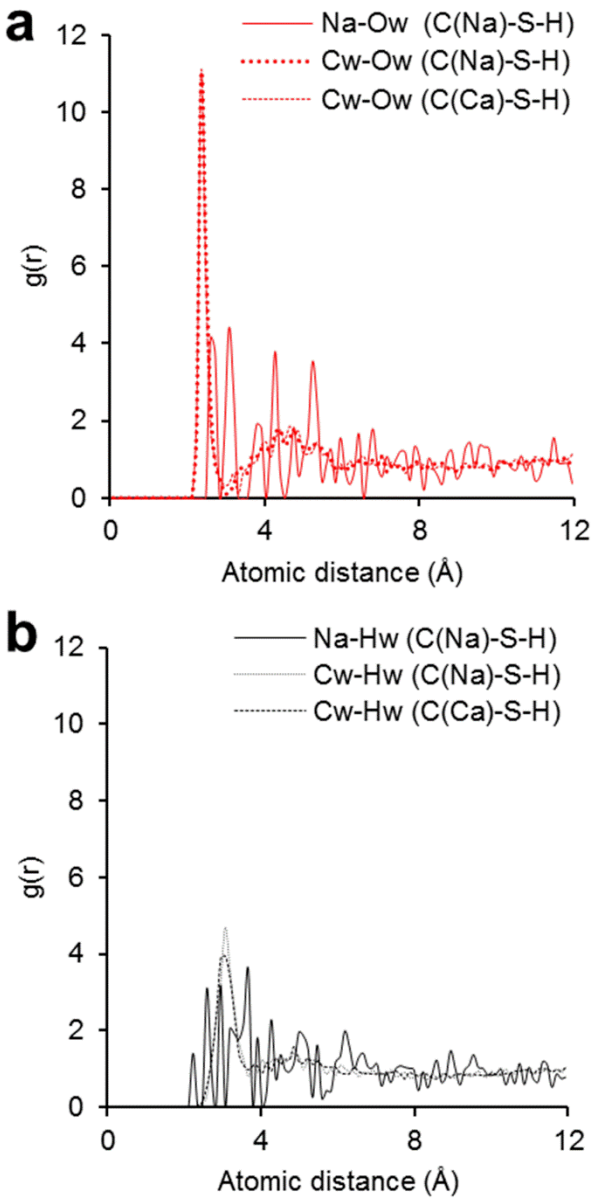


Figure 14. Radial distribution function of (a) oxygen (Ow) and (b) hydrogen (Hw) from the water molecules with sodium (Na) and calcium (Cw) cations in the interlayer of C-S-$H_{layer}$ for C(Na)-S-H and C(Ca)-S-H.

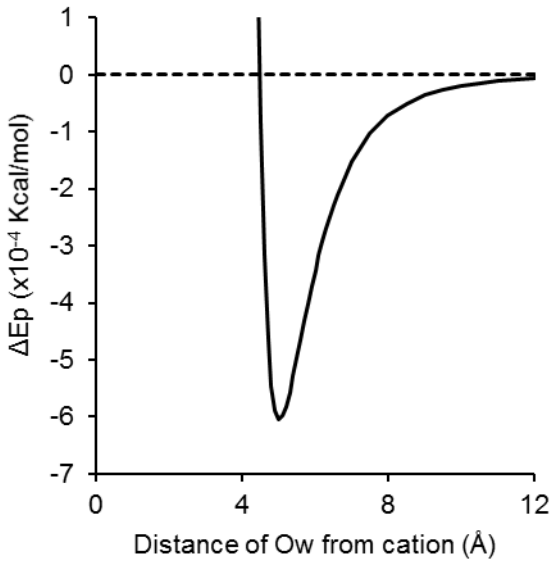


Figure 15. Potential-energy difference (ΔEp) of the interactions between two sodium cations and oxygen from the water molecules (2Na-Ow) and calcium cations and oxygen from the water molecules (Ca-Ow). The negative ΔEp indicates the greater attractive potential-energy of 2Na-Ow compared to Ca-Ow, thus indicating the relatively stronger 2Na-Ow interaction. The infinitively increasing distance of Ow from Na or Ca results in negative ΔEp approaching 0.

$Na^+$ incorporation also influenced the lateral deformation of the C-S-$H_{layer}$, which decreased under compressive loading along the longitudinal (z) direction, as shown in Figure 16. In contrast, the lateral deformation increased under tensile loading. The changes in lateral deformations were attributed to the additionally attractive effect of $Na^+$ on water molecule. Under compressive loading, the attractive $Na^+$ resisted the expansive lateral deformation. On the other hand, the attractive $Na^+$ enhanced the contractive lateral deformation under tensile loading. The higher attractive $Na^+$ could be due to the exchange of two $Na^+$ for one calcium cation, which resulted in an additional stiffening effect within the interlayer of C-S-$H_{layer}$ and influenced its lateral deformability.

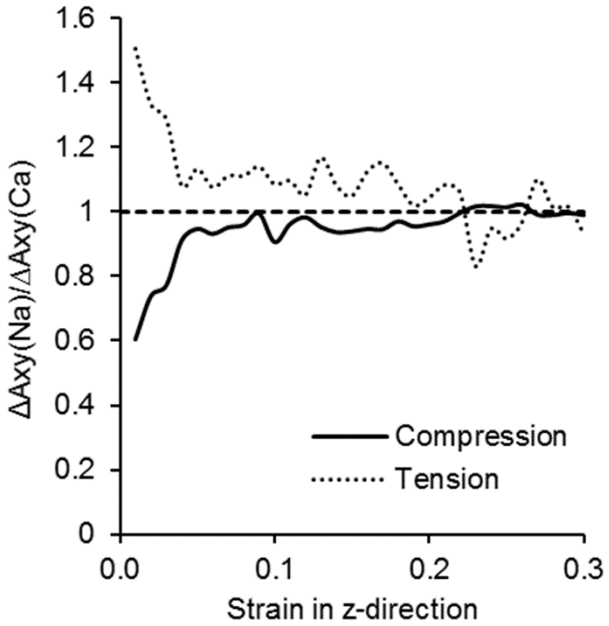


Figure 16. Ratio of lateral deformation in C(Na)-S-H and C(Ca)-S-H system under compressive and tensile loadings along the perpendicular direction of the C-S-H layers. ΔAxy(Na)/ΔAxy(Ca) expresses the comparative lateral contraction and expansion between C(Na)-S-H and C(Ca)-S-H under compressive and tensile loading along z-direction, respectively.

The results from this study revealed that the effect of $Na^+$ incorporation on the mechanical properties of C-S-$H_{layer}$ originated from $Na^+$ interaction with the water molecules. A greater water attracting effect was seen with the replacement of one calcium by two $Na^+$ ions in the interlayer of C-S-$H_{layer}$ compared to without the presence of $Na^+$. The greater cationic attraction by $Na^+$ was indicated by a reduction in the lateral dimension of C-S-$H_{layer}$ and was manifested by a stiffening of the interlayer (i.e., the layer with the water molecules) that, in turn, resulted in a lower per-atom average stress of the calcium cations in the intralayer of C-S-$H_{layer}$. The effect of $Na^+$ incorporation on the mechanical properties of C-S-$H_{layer}$ was found, however, to be statistically insignificant.

# 4. Conclusions

In this study, the Young's modulus and strength of C-S-$H_{layer}$ with and without $Na^+$ (i.e., C(Na)-S-H and C(Ca)-S-H, respectively) was examined based on the response to tensile and compressive loadings from the direction that was either perpendicular (i.e., z-direction) or parallel (i.e., xy-direction) to the C-S-$H_{layer}$ stacked layers. The effect of $Na^+$ on the mechanical properties

of C-S-$H_{layer}$ was found to be statistically insignificant. This result suggested that the effect of sodium commonly reported in the literature on the mechanical properties of hydrated cement most likely did not originate from the atomic level of C-S-$H_{layer}$. It is thus suggested that future investigations of the effect of sodium containing compounds on the mechanical properties of hydrated cement should focus on the higher scale structure of C-S-H (e.g., interaction of C-S-H nanoparticles).

Based on the atomic internal response to the externally applied loads, the C-S-$H_{layer}$ model could be simplified into a bilayer composite. The atoms in the interlayer transferred the externally applied loads. In contrast, the atoms in the intralayer stiffened the structure and resisted the movement of water along the lateral deformation. In the case of C-S-$H_{layer}$ incorporating $Na^+$, the presence of $Na^+$ provided an additional water attracting effect, which was thought to result from the exchange of two $Na^+$ for one calcium cation (i.e., greater total hydration number). The findings obtained in this study provide useful information that should be considered in the fundamental study of the effect of saline environment on the properties of cement-based materials.

## Declaration of Competing Interest

None.

## Acknowledgement

The authors would like to acknowdge the finanical support of the Hong Kong Research Grants Council Theme Based Reserch Scheme.

## References

[1] A. Kumar, G. Sant, C. Patapy, C. Gianocca, K.L. Scrivener, The influence of sodium and potassium hydroxide on alite hydration: Experiments and simulations, Cement and Concrete Research 42(11) (2012) 1513-1523.

[2] M.C.G. Juenger, H.M. Jennings, Examining the relationship between the microstructure of calcium silicate hydrate and drying shrinkage of cement pastes, Cement and Concrete Research 32(2) (2002) 289-296.

[3] D.E. Macphee, K. Luke, F.P. Glasser, E.E. Lachowski, Solubility and aging of calcium silicate hydrates in alkaline solutions at 25 C, Journal of the American Ceramic Society 72(4) (1989) 646-654.
[4] I. Jawed, J. Skalny, Alkalies in cement: a review: II. Effects of alkalies on hydration and performance of Portland cement, Cement and concrete research 8(1) (1978) 37-51.
[5] B. Mota, T. Matschei, K. Scrivener, Impact of NaOH and Na 2 SO 4 on the kinetics and microstructural development of white cement hydration, Cement and Concrete Research 108 (2018) 172-185.
[6] B. Mota, T. Matschei, K. Scrivener, Impact of sodium gluconate on white cement-slag systems with Na2SO4, Cement and Concrete Research 122 (2019) 59-71.
[7] B. Mota, T. Matschei, K. Scrivener, The influence of sodium salts and gypsum on alite hydration, Cement and Concrete Research 75 (2015) 53-65.
[8] A. Cuesta, J.D. Zea-Garcia, D. Londono-Zuluaga, G. Angeles, I. Santacruz, O. Vallcorba, M. Dapiaggi, S.G. Sanfélix, M.A. Aranda, Multiscale understanding of tricalcium silicate hydration reactions, Scientific reports 8(1) (2018) 8544.
[9] H.M. Jennings, Refinements to colloid model of CSH in cement: CM-II, Cement and Concrete Research 38(3) (2008) 275-289.
[10] H.M. Jennings, A model for the microstructure of calcium silicate hydrate in cement paste, Cement and concrete research 30(1) (2000) 101-116.
[11] M.J. Sánchez-Herrero, A. Fernández-Jiménez, A. Palomo, C3S and C2S hydration in the presence of Na2CO3 and Na2SO4, Journal of the American Ceramic Society 100(7) (2017) 3188-3198.
[12] D. Sugiyama, Chemical alteration of calcium silicate hydrate (C–S–H) in sodium chloride solution, Cement and Concrete Research 38(11) (2008) 1270-1275.
[13] M.J. Sánchez-Herrero, A. Fernández-Jiménez, Á. Palomo, Alkaline hydration of C2S and C3S, Journal of the American Ceramic Society 99(2) (2016) 604-611.
[14] T. Zhou, K. Ioannidou, F.-J. Ulm, M.Z. Bazant, R.-M. Pellenq, Multiscale poromechanics of wet cement paste, Proceedings of the National Academy of Sciences 116(22) (2019) 10652-10657.

[15] Y. Zha, J. Yu, R. Wang, P. He, Z. Cao, Effect of ion chelating agent on self-healing performance of Cement-based materials, Construction and Building Materials 190 (2018) 308-316.
[16] W. Li, S. Kawashima, J. Xiao, D.J. Corr, C. Shi, S.P. Shah, Comparative investigation on nanomechanical properties of hardened cement paste, Materials and Structures 49(5) (2016) 1591-1604.
[17] W. Ashraf, J. Olek, N. Tian, Multiscale characterization of carbonated wollastonite paste and application of homogenization schemes to predict its effective elastic modulus, Cement and Concrete Composites 72 (2016) 284-298.
[18] D. Hou, Y. Zhu, Y. Lu, Z. Li, Mechanical properties of calcium silicate hydrate (C–S–H) at nano-scale: a molecular dynamics study, Materials Chemistry and Physics 146(3) (2014) 503-511.
[19] F. Sanchez, K. Sobolev, Nanotechnology in concrete–a review, Construction and building materials 24(11) (2010) 2060-2071.
[20] X.Q. Wang, C.L. Chow, D. Lau, A Review on Modeling Techniques of Cementitious Materials under Different Length Scales: Development and Future Prospects, Advanced Theory and Simulations 1900047.
[21] D. Lau, W. Jian, Z. Yu, D. Hui, Nano-engineering of construction materials using molecular dynamics simulations: Prospects and challenges, Composites Part B: Engineering 143 (2018) 282-291.
[22] J.J. Biernacki, J.W. Bullard, G. Sant, K. Brown, F.P. Glasser, S. Jones, T. Ley, R. Livingston, L. Nicoleau, J. Olek, Cements in the 21st century: challenges, perspectives, and opportunities, Journal of the American Ceramic Society 100(7) (2017) 2746-2773.
[23] H. Liu, S. Dong, L. Tang, N.A. Krishnan, G. Sant, M. Bauchy, Effects of polydispersity and disorder on the mechanical properties of hydrated silicate gels, Journal of the Mechanics and Physics of Solids 122 (2019) 555-565.
[24] J. Fu, S. Kamali-Bernard, F. Bernard, M. Cornen, Comparison of mechanical properties of CSH and portlandite between nano-indentation experiments and a modeling approach using various simulation techniques, Composites Part B: Engineering 151 (2018) 127-138.

[25] A. Dufresne, J. Arayro, T. Zhou, K. Ioannidou, F.-J. Ulm, R. Pellenq, L.K. Béland, Atomistic and mesoscale simulation of sodium and potassium adsorption in cement paste, The Journal of chemical physics 149(7) (2018) 074705.
[26] R.J.-M. Pellenq, A. Kushima, R. Shahsavari, K.J. Van Vliet, M.J. Buehler, S. Yip, F.-J. Ulm, A realistic molecular model of cement hydrates, Proceedings of the National Academy of Sciences 106(38) (2009) 16102-16107.
[27] X. Cong, R.J. Kirkpatrick, 29Si MAS NMR study of the structure of calcium silicate hydrate, Advanced Cement Based Materials 3(3-4) (1996) 144-156.
[28] A. Ayuela, J.S. Dolado, I. Campillo, Y. De Miguel, E. Erkizia, D. Sánchez-Portal, A. Rubio, A. Porro, P.M. Echenique, Silicate chain formation in the nanostructure of cement-based materials, The Journal of chemical physics 127(16) (2007) 164710.
[29] A.J. Allen, J.J. Thomas, H.M. Jennings, Composition and density of nanoscale calcium–silicate–hydrate in cement, Nature materials 6(4) (2007) 311.
[30] R. Shahsavari, R.J.-M. Pellenq, F.-J. Ulm, Empirical force fields for complex hydrated calcio-silicate layered materials, Physical Chemistry Chemical Physics 13(3) (2011) 1002-1011.
[31] R.T. Cygan, J.-J. Liang, A.G. Kalinichev, Molecular models of hydroxide, oxyhydroxide, and clay phases and the development of a general force field, The Journal of Physical Chemistry B 108(4) (2004) 1255-1266.
[32] M.J.A. Qomi, F.-J. Ulm, R.J.-M. Pellenq, Physical origins of thermal properties of cement paste, Physical Review Applied 3(6) (2015) 064010.
[33] M.J.A. Qomi, M. Bauchy, F.-J. Ulm, R.J.-M. Pellenq, Anomalous composition-dependent dynamics of nanoconfined water in the interlayer of disordered calcium-silicates, The Journal of chemical physics 140(5) (2014) 054515.
[34] M. Bauchy, M.A. Qomi, F.-J. Ulm, R.-M. Pellenq, Order and disorder in calcium–silicate–hydrate, The Journal of chemical physics 140(21) (2014) 214503.
[35] M.A. Qomi, K. Krakowiak, M. Bauchy, K. Stewart, R. Shahsavari, D. Jagannathan, D.B. Brommer, A. Baronnet, M.J. Buehler, S. Yip, Combinatorial molecular optimization of cement hydrates, Nature communications 5 (2014) 4960.
[36] S. Plimpton, Fast parallel algorithms for short-range molecular dynamics, Journal of computational physics 117(1) (1995) 1-19.

564 [37] W.G. Hoover, Constant-pressure equations of motion, Physical Review A 34(3) (1986)
565 2499.
566 [38] W.G. Hoover, Canonical dynamics: Equilibrium phase-space distributions, Physical review
567 A 31(3) (1985) 1695.
568 [39] D.J. Evans, B.L. Holian, The nose–hoover thermostat, The Journal of chemical physics
569 83(8) (1985) 4069-4074.
570 [40] J. Kolafa, J.W. Perram, Cutoff errors in the Ewald summation formulae for point charge
571 systems, Molecular Simulation 9(5) (1992) 351-368.
572 [41] D. Hou, H. Ma, Y. Zhu, Z. Li, Calcium silicate hydrate from dry to saturated state:
573 structure, dynamics and mechanical properties, Acta materialia 67 (2014) 81-94.
574 [42] B. Al-Muhit, F. Sanchez, Tunable mechanical properties of graphene by clustered line
575 pattern hydroxyl functionalization via molecular dynamics simulations, Carbon 146 (2019)
576 680-700.
577 [43] A.P. Thompson, S.J. Plimpton, W. Mattson, General formulation of pressure and stress
578 tensor for arbitrary many-body interaction potentials under periodic boundary conditions,
579 The Journal of chemical physics 131(15) (2009) 154107.
580 [44] C.H. Rycroft, G.S. Grest, J.W. Landry, M.Z. Bazant, Analysis of granular flow in a pebble-
581 bed nuclear reactor, Physical review E 74(2) (2006) 021306.
582 [45] D.M. Heyes, Pressure tensor of partial-charge and point-dipole lattices with bulk and
583 surface geometries, Physical Review B 49(2) (1994) 755.
584 [46] H. Dramé, J. Beaudoin, L. Raki, A comparative study of the volume stability of C–S–H (I)
585 and Portland cement paste in aqueous salt solutions, Journal of materials science 42(16)
586 (2007) 6837-6846.
587 [47] J.A. White, E. Schwegler, G. Galli, F. Gygi, The solvation of Na+ in water: First-principles
588 simulations, The Journal of Chemical Physics 113(11) (2000) 4668-4673.
589 [48] Z. Yu, A. Zhou, D. Lau, Mesoscopic packing of disk-like building blocks in calcium
590 silicate hydrate, Scientific reports 6 (2016) 36967.
591 [49] O. Mendoza, C. Giraldo, S.S. Camargo Jr, J.I. Tobón, Structural and nano-mechanical
592 properties of Calcium Silicate Hydrate (CSH) formed from alite hydration in the presence
593 of sodium and potassium hydroxide, Cement and Concrete Research 74 (2015) 88-94.

[50] J. Wang, E. Liu, L. Li, Multiscale investigations on hydration mechanisms in seawater OPC paste, Construction and Building Materials 191 (2018) 891-903.
[51] L. Brown, P.G. Allison, F. Sanchez, Use of nanoindentation phase characterization and homogenization to estimate the elastic modulus of heterogeneously decalcified cement pastes, Materials & Design 142 (2018) 308-318.
[52] D. Hou, H. Li, L. Zhang, J. Zhang, Nano-scale mechanical properties investigation of CSH from hydrated tri-calcium silicate by nano-indentation and molecular dynamics simulation, Construction and Building Materials 189 (2018) 265-275.
[53] D. Fan, S. Yang, Mechanical properties of CSH globules and interfaces by molecular dynamics simulation, Construction and Building Materials 176 (2018) 573-582.
[54] A. Zhou, R. Qin, C.L. Chow, D. Lau, Structural performance of FRP confined seawater concrete columns under chloride environment, Composite Structures 216 (2019) 12-19.
[55] Y.L. Yaphary, Z. Yu, R.H. Lam, D. Hui, D. Lau, Molecular dynamics simulations on adhesion of epoxy-silica interface in salt environment, Composites Part B: Engineering 131 (2017) 165-172.
[56] A.K. Katz, J.P. Glusker, S.A. Beebe, C.W. Bock, Calcium ion coordination: a comparison with that of beryllium, magnesium, and zinc, Journal of the American Chemical Society 118(24) (1996) 5752-5763.
[57] S. Weerasinghe, P.E. Smith, A Kirkwood–Buff derived force field for sodium chloride in water, The Journal of chemical physics 119(21) (2003) 11342-11349.
[58] J.N. Israelachvili, Intermolecular and surface forces, Academic press2011.